PCCP

Cite this: *Phys. Chem. Chem. Phys.*, 2012, **14**, 13370–13377

www.rsc.org/pccp

PAPER

Photoexcitation of mass/charge selected hemin$^+$, caught in helium nanodroplets

Frank Filsinger,* Doo-Sik Ahn, Gerard Meijer and Gert von Helden*

Received 20th June 2012, Accepted 9th August 2012
DOI: 10.1039/c2cp42071f

We report on a method by which mass/charge selected ions are picked up from a linear ion trap by liquid helium droplets. The size distributions of the doped droplets are measured *via* acceleration experiments. Depending on the source temperature, droplet sizes ranging from tens of thousands to several million helium atoms are obtained. Droplets doped with hemin, an iron containing porphyrin molecule, in the charge state +1 are then investigated using laser spectroscopy. It is observed that excitation with UV/VIS light can lead to ejection of the ion from the droplet. For doped droplets with a median size of ~150 000 helium atoms, the absorption of two photons at 380 nm is needed for ejection to become efficient. When droplets become smaller, the ejection efficiency is observed to strongly increase. Monitoring the ejection yield as a function of excitation wavelength can be used to obtain the optical spectrum of hemin$^+$. Compared to the spectrum of free gas-phase hemin$^+$ at room temperature, the here obtained spectrum is slightly narrower and shifted to the blue.

1 Introduction

Liquid helium can serve as a unique matrix to study embedded molecules or clusters. It is difficult, however, to use bulk liquid helium, as dopant molecules will aggregate or diffuse to the container walls and furthermore, sensitive spectroscopic methods are difficult to apply. A breakthrough occurred with the advent of liquid helium droplet methods[1] that allow for controlled doping and the application of highly sensitive spectroscopic methods.[2,3] Since then, this technique has been exploited in many studies.[4–7] The experiments show that even small liquid helium droplets have an equilibrium temperature of only 0.38 K, are superfluid and can allow for nearly free rotation of the dopant molecules.[8,9] In most experiments, a droplet beam is generated by the expansion of cold helium gas into vacuum followed by the pickup of evaporated species in a pickup-cell. Using this scheme, a wide variety of neutral species, such as atoms,[10,11] small molecules[2] and biomolecules[12] as well as larger molecules, such as C_{60}[13] and clusters,[14] can be embedded in helium droplets. For droplet production, continuous[1–7] or recently also pulsed[15,16] expansions of cold helium gas are used. Especially pulsed expansions have been shown to be very useful, as they provide for high peak intensities while minimizing pumping requirements and further, their time structure can be well matched to that of standard pulsed laser systems.

Doped droplets are very often used in spectroscopy experiments and numerous atom, molecules and cluster doped droplets have been studied so far.[4] When performing electronic spectroscopy on larger organic molecules in helium droplets, it is observed that the spectra of many molecules consist of sharp lines followed by a phonon wing.[17] When, however, the excited state involves a geometry change, spectra can become broad.[17] This is especially the case for electronic spectra of ionic species in helium droplets.[18] In those experiments ion-doped droplets are produced by photoionization of initially neutral droplets, which are then investigated using electronic and vibrational spectroscopy.[18–20] It is observed that upon photoexcitation, ejection of the charged particle from the droplet can occur.[19] This is surprising, as by any statistical argument, the evaporation of neutral helium atoms and not the ejection of the presumably much more strongly bound ion should occur. The important role of non-thermal, non-statistical cooling processes has been investigated both experimentally[21] and theoretically[22] before. However, an understanding of the underlying mechanisms is still lacking.

A general drawback of the standard pickup technique is that it is limited to species that can either be thermally evaporated or laser vaporized. This is not possible for many species such as for example larger biomolecules which would decompose under such conditions. An additional complication arises when the dopant molecules are only available in very low densities. Helium droplets have the property that they pick up almost everything on their path. When the following measurement and/or detection steps are not selective for the dopant species, the resulting signal might be obscured by everything the droplets have picked up.

We have recently introduced a pickup method that circumvents those problems. In this technique,[23] the standard pickup

Fritz-Haber-Institut der Max-Planck-Gesellschaft, Faradayweg 4-6, 14195 Berlin, Germany. E-mail: helden@fhi-berlin.mpg.de

cell is replaced by a linear radio frequency (RF) ion trap, which is loaded with mass/charge selected ions. For performing experiments on biomolecules, those ions can, for example, be brought into the gas phase *via* electrospray ionization (ESI). In the ion trap, the ions are confined in directions perpendicular to the droplet beam by the RF field. In the longitudinal direction, trapping is achieved by applying a low electrical potential to the endcap electrodes of the trap. Due to their high mass, the kinetic energy of the droplets from the source is much higher than this trapping potential and droplets that have picked up an ion can thus continue to fly in the beam direction and travel out of the trap. The doped droplets can then be interrogated using for example lasers and detection can be performed using standard charged particle detection methods that can have sensitivities up to individual particle counting. As those techniques are only sensitive to charged particles, all droplets that picked up residual gas but not ions will not give rise to any signal. Of course, some droplets will have picked up both residual gas as well as charged particles, which might give rise to spurious signals. However, the amount of those droplets will be much less than the amount of droplets that have picked up only one species (provided that the doping probability for either step is less than unity).

In many experiments, the droplet size is a critical parameter. For continuous sources, the droplet size distributions have been measured *via* deflection experiments,[24] acceleration of droplets after electron[25] or ion[11] capture or the attenuation in a scattering cell.[26] For pulsed sources, mean droplet sizes were estimated by monitoring fluorescence from dopant species[15] and Rayleigh scattering.[16] Acceleration experiments on charged droplets offer the advantage of being very sensitive and further, of being able to measure not only the mean size but also the shape of the size distribution. When the charge comes from a single electron,[25] a metastable electron bubble is formed and the efficiency of electron capture as well as the lifetime of the charged droplet will depend on droplet size. On the other hand, when charging by ion capture occurs and the ion is sufficiently small, stable doped droplets are expected to form and the capture probability only depends on the droplet size.

Here, we present a study on hemin, an iron containing porphyrin molecule, as a singly charged ion in helium droplets. In the first part, the size distribution as a function of droplet source temperature is investigated. In the second part, the doped droplets are exposed to UV/VIS light, probing the Soret band of hemin around 380 nm.

2 Experimental setup

A scheme of the experiment is shown in Fig. 1. It is similar to a setup described before,[23] however differs in several important aspects. The front-end of the setup stems from a commercial Waters QTof Ultima mass spectrometer in which most electrical and electronic parts are substituted by custom-made components. Ions are brought into the gas phase *via* electrospray ionization. After passing through two differentially pumped ion guides, mass/charge selection takes place in a quadrupole mass spectrometer. The continuous ion beam is then bent by 90° using a quadrupole bender and injected into a 30 cm long linear hexapole ion trap. This trap, which consists of six 5 mm diameter stainless steel rods that are placed on

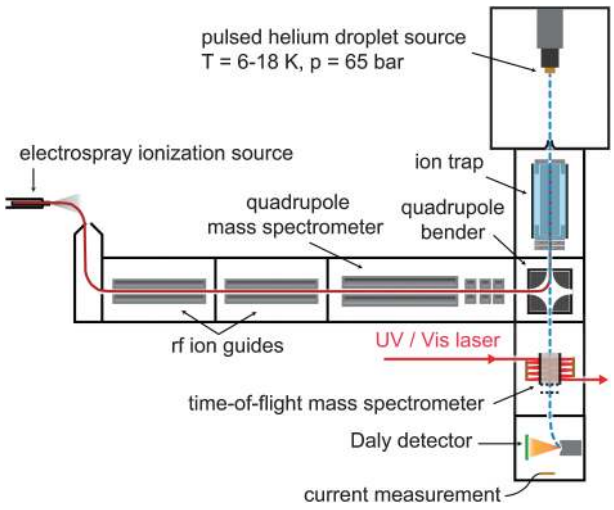

Fig. 1 Schematic depiction of the experimental setup. Biomolecules are brought into the gas phase using electrospray ionization, are mass/charge selected and are stored in an ion trap, from which they are picked up by a pulsed beam of helium droplets. The doped droplets travel straight through the then grounded quadrupole bender and can be interrogated using laser light.

a 14.1 mm diameter circle, is operated with 1.7 MHz radio frequency for the radial confinement of the ions. Two endcap electrodes that are kept a few volts above the dc potential of the rods provide the longitudinal trapping potential. During trap loading, pulses of He buffer gas are injected into the trap so that incoming ions with a kinetic energy just above the endcap potential will lose some energy *via* collisions with the buffer gas and will be stored in the trap. After loading for a few seconds, the space charge limit ($\sim 10^6$–10^7 elementary charges per cm^3) in the trap is reached, the trap loading is stopped, and the buffer gas is pumped away. In the second time interval of the experimental sequence, during which the actual helium droplet experiments are performed, the helium droplet beam is pulsed through the trap. The helium droplet source consists of a cryogenic Even–Lavie pulsed valve[16] that is mounted on the second stage of a closed cycle cryostat (Sumitomo RDK 408D2). In the experiments presented here, the pulsed valve is operated at source temperatures between 6 K and 18 K and a stagnation pressure p_0 of 65 bar. It emits $\sim$30 μs long pulses of helium droplets at repetition rates of up to 50 Hz (limited by the pumping capacity in the source chamber). The forward direction of the helium droplet beam defines the positive z-direction and the valve is located at $z = 0$. Before entering the trapping chamber, the helium droplet beam is skimmed using a 4 mm diameter skimmer (Beam Dynamics Model 50.8) at $z = 13.5$ cm. Upon traversing the ion trap, a droplet can pick up an ion *via* mechanical impact. Because the droplets are very heavy and the kinetic energy of the doped droplet exceeds the longitudinal trapping potential, the ion can leave the trap inside the droplet. As the ions are otherwise stably confined in the trap, the transport in a helium droplet is the only significant escape route for ions. The ion-doped droplets then pass through the (then grounded) bender and can be analyzed and manipulated further downstream. When the droplet beam has depleted the trap content by $\sim$50%

(after about 1 minute), the helium droplet source is stopped and the experimental sequence is re-started by re-loading the trap. An additional TOF mass spectrometer is mounted on the free arm of the quadrupole bender (not shown in Fig. 1). It allows for analysis of the trap contents to ensure that the ions in the trap have not fragmented or reacted with background gas during storage. All TOF mass spectrometers operate with pulsed extraction fields.

Two detectors can alternatively be used to monitor the droplet beam. The first detector consists of a Faraday cup at $z = 2.02$ m, connected to a calibrated current-to-voltage amplifier (Femto DLPCA-200). The advantage of this detector is that it provides the true ion current and that the detection efficiency does not depend on the mass. Therefore, the Faraday cup is used in all experiments, where the size of the doped droplets is investigated. However, the disadvantage of this detection method is that the peak currents are small (typically <1 pA) and therefore the signal-to-noise ratio is rather poor. Alternatively, the doped droplets can be measured using a Daly-type detector. For this, the droplets pass through a grounded circular aperture (12 mm diameter, located at $z = 1.71$ m), before they are accelerated towards a polished aluminum high-voltage electrode at -20 kV that is placed off-axis. Upon impact on the aluminum surface, secondary electrons can be produced which are detected using an electron multiplier opposing the aluminum electrode. This detection method yields a 100-fold better signal-to-noise ratio compared to the direct current measurement. However, in contrast to the direct current measurements, the sensitivity of this detection method depends in an unknown way on the droplet mass.

For spectroscopic investigations, the helium droplets are intersected by a pulsed dye laser beam at a 90° incidence angle at $z = 1.33$ m. The laser emits $\sim$5 ns long pulses at wavelengths around 380 nm with an energy of up to 5 mJ per pulse and has a bandwidth of 0.04 cm^{-1}. To irradiate almost the whole droplet beam, which has a spatial length of $\sim$4 cm in the interaction region, a multipass cell can be used. This multipass cell consists of two right-angle prisms and enables seven passes of the same laser pulse through the droplet beam. Two different time-of-flight mass spectrometers are available to monitor the charged particles after irradiation with the laser light. In the first spectrometer, the particles are accelerated along the positive z-direction towards the Daly detector. This spectrometer is used to detect changes in the size distribution of the helium droplets induced by the laser light. The mass resolution in this setup is limited by the temporal width of the helium droplet pulse. The second spectrometer (not shown in Fig. 1) allows for extraction of ions in the direction perpendicular to the propagation direction of the helium droplets and is mounted where the laser beam crosses the droplet beam. This spectrometer is equipped with a multichannel plate (MCP) detector, has a mass resolution of $\sim$100, and is used to detect any small ions that are generated after laser irradiation. This TOF is equipped with deflection electrodes to compensate for the kinetic energy in the original droplet flight direction. However, as the droplet beam moves with a constant velocity, the spread of kinetic energies is large and only a limited mass range can be brought on the MCP (*i.e.* doped droplets and small ions can not be detected at the same time).

3 Results and discussion

3.1 Droplet size determination

To measure the size distributions of the doped droplets, time-of-flight mass spectrometry with signal detection on the Faraday cup detector is performed. In those experiments, the trap bias is raised to a voltage U_{acc} after loading of the trap is completed. When ion-doped droplets then exit the trap, they are accelerated by U_{acc} towards ground potential between two electrodes equipped with grids, just outside the trap. This is schematically shown in Fig. 2(A). In Fig. 2(B), time profiles are shown that are obtained when the trap is loaded with $hemin^+$ and the droplet source is operated at $T_{source} = 14$ K with 65 bar of helium backing pressure at a repetition rate of 20 Hz. In the bottom trace of Fig. 2(B), the time profile of the unaccelerated beam is shown. This time profile can be fitted with a Gaussian velocity distribution (solid line) and a mean velocity of 405 m s^{-1} with a full width at half maximum (FWHM) of 4 m s^{-1} is obtained for this case. Under the experimental conditions employed in the present study, the measured peak currents at 0 U_{acc} acceleration are $\sim$0.6 pA at $T_{source} = 6.3$ K, increasing to values of 0.7–0.9 pA at temperatures between 10 K and 14 K and then decreasing to 0.4 pA at 16 K and 0.2 pA up to 18 K. Above 18 K, the signal is too weak to perform measurements using the Faraday cup detector. Time profiles for $U_{acc} = 50$ V, 100 V and 300 V for $T_{source} = 14$ K are shown in the upper three traces. Clearly, the profiles shift to shorter times and also broaden, as the droplets do not have a single mass but a broad mass distribution. Cluster and droplet size distributions can often be well described by log-normal distributions,

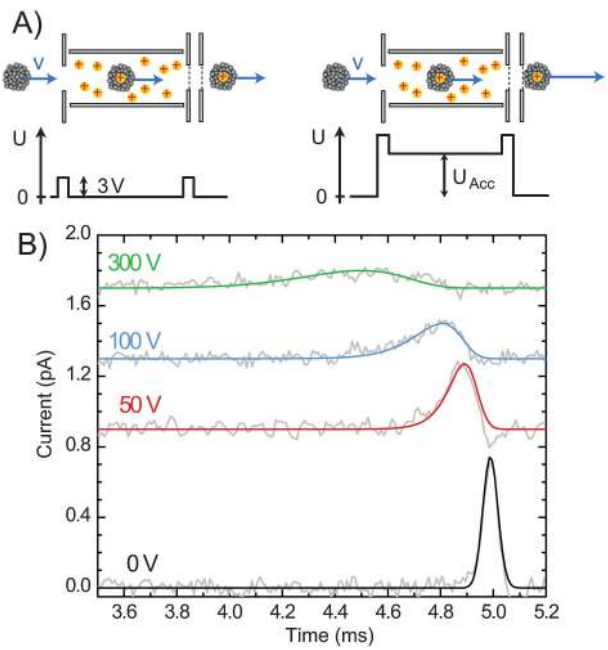

Fig. 2 (A) Scheme of the acceleration experiment to determine the droplet size distributions. First, ions are loaded into the trap. When the DC level of the RF (U_{acc}) is raised, doped droplets are accelerated after exiting the trap. (B) Time profiles of accelerated droplets. Shown as solid lines is a fit to TOF profiles resulting from a log-normal droplet size distribution.

i.e. Gaussian distributions on a logarithmic scale whose probability density distribution is given by eqn (1).

$$P(n) = \frac{1}{n\sigma\sqrt{2\pi}} e^{-\frac{(\ln n-\mu)^2}{2\sigma^2}} \quad (1)$$

Log-normal distributions are described by the position parameter μ and the width parameter σ. The ion-capture process will have an influence on the observed distribution. As a first approximation, the capture probability will scale the geometric collision cross-section, *i.e.* scale with $n^{2/3}$. As can be easily shown, a multiplication of eqn (1) with $n^{2/3}$ results in a new log-normal distribution, having an unchanged parameter σ however a new position parameter μ', which is given by $\mu' = \mu + \frac{2}{3}\sigma^2$. Time profiles of accelerated droplets and their fits with those expected for a log-normal distribution are shown in Fig. 2(B). In those fits μ and σ are the fit parameters. They depend on the source temperature and are constant for a given source temperature and different acceleration voltages. The resulting fitted distributions for T_{source} = 14 K and 17 K for 65 bar backing pressure are shown in the top part of Fig. 3. The maximum (mode) of a log-normal distribution is given by $e^{(\mu-\sigma^2)}$. However, as the distribution is very asymmetric, the median of the distribution, given by e^{μ}, is sometimes a more useful parameter to describe its shape.

In the bottom part of Fig. 3, the parameters of the fitted distribution are plotted as a function of T_{source}. The medians of the distributions are shown as circles and the modes of the distributions as squares. The bars cover the ranges between the half heights of the distributions. As expected, lowering the temperature shifts the distribution to larger droplets and adjusting the temperature allows for tuning the distributions from a median of about 83 000 helium atoms at 18 K to about 1.6 million helium atoms near 6 K. At the same time, the widths of the distributions increase. At the high temperatures of 17 and 18 K, however, the signal-to-noise in the measurements becomes worse and the uncertainty in the determination of the width and position becomes high. The data for those temperatures thus rather represent a general trend. The size determinations presented here have been performed over the course of a couple of weeks with the valve kept constantly at low temperatures and at a valve repetition rate of 20 Hz. Under those conditions, the day to day obtained values of the medians of the distributions varied by not more than 10%. From the observed distributions for the doped droplets, the distributions of the undoped droplets can be estimated by taking into account the above mentioned $n^{2/3}$ collision cross-section dependence. For the widest distributions at low temperatures, the median of the undoped distribution is expected to be smaller by a factor of 0.67 and for the narrowest distributions at high temperatures, the median is reduced by a factor of 0.94.

Size distributions were also measured at higher pulsed valve repetition rates and also for different ionic species, such as the atomic ion Cs^+, the protonated aminoacid tryptophan-H^+ as well as several larger peptides and proteins. Results will be reported upon elsewhere.[27] It is observed that when the ion is comparatively small (molecular weight $< \sim 1000$ u), the observed droplet distributions are essentially not affected by

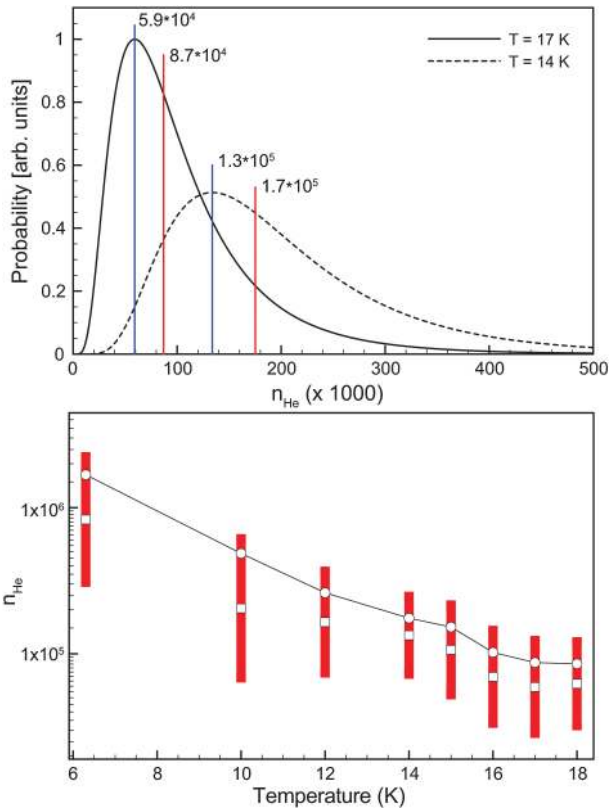

Fig. 3 Top: fitted droplet size distributions for T_{source} = 14 K and 17 K. The positions of the modes and medians of the distributions are indicated. (B) Parameters of fitted size distributions as a function of T_{source}. Circles indicate the medians and squares the modes of the distributions. The bars represent the ranges between the half height of the distributions.

the type of ion. On the other hand, several experimental parameters can have an influence on the observed distributions. When, for example, at one point after many weeks of operation at low temperature, the valve was warmed up to room temperature and re-cooled to low temperature, the observed medians increased by up to a factor of three. The reason for this is likely the slow but steady freezing out of gases at the exit orifice, effectively reducing its opening size over time. Similarly, when we replaced after finishing the present study the Kapton sealing gasket that, with its 60 μm opening, defines the nozzle orifice diameter, the distributions also changed and, for temperatures below 16 K, became strongly bi-modal. It should be pointed out, however, that this is most probably not only a problem for our setup, and that it can actually be very important to be able to determine the droplet sizes on a regular basis.

Thus, it can be difficult to compare size distributions from different experiments, even when they are measured under nominally similar conditions. This is underlined by comparing the here obtained results to those of a previous study where we reported upon droplets that are larger by more than six orders of magnitude.[23] In that study, we employed a different pulsed valve with a different nozzle geometry and nozzle opening (800 μm previously, 60 μm in the present study). Nonetheless, it is difficult to rationalize those differences using accepted scaling rules.[28]

It should however also be mentioned that the droplet sizes determined here are in qualitative agreement with estimates obtained by others using a very similar pulsed valve.[16]

3.2 Laser excitation

The procedure to perform spectroscopy on mass/charge selected ions in helium droplets is described in the experimental section and depicted in Fig. 1. In a first experiment, the droplet beam is irradiated using the multipass optical setup. Detection is performed using the Daly detector. In the top trace of Fig. 4, the time profile of the unaccelerated droplet beam at a source temperature of 16 K with the excitation laser turned off is shown. The resulting beam velocity is 410 m s^{-1}. When the laser interaction region is pulsed to +50 V after the droplets have entered, but the laser has not fired, droplets that are exiting the interaction region are accelerated and the shifted time profile (b) is measured. The maximum of the ion cloud exits the laser interaction region (to be then accelerated) at t_0 = 3.4 ms. The observed shift of the peak in (b) is in line with a median droplet size of 1×10^5 helium atoms. When the droplet beam is in addition overlapped with the pulsed laser beam at 382 nm, the time profile shown in (c) is measured. The subtraction of (b) and (c) is shown in (d). Clearly, the main peak in (c) is not measurably shifted from its original position in (b). One 382 nm photon carries enough energy to potentially cause the evaporation of about 5300 helium atoms (assuming a helium atom binding energy of 5 cm^{-1}).[6] When one compares this number to the median of the droplet size, takes into account the width of the distribution and considers the inherent low resolution of the here employed TOF setup, it becomes clear that if one photon would cause the shrinkage of a droplet, it would not be detectable in the current experimental scheme. Observed is, however, the appearance of an additional peak at earlier times. The position of this peak is where one would expect bare hemin$^+$ to appear. For hemin$^+$ to appear from a complete evaporation of its helium solvation shell, the absorption of about 20 photons at 382 nm is required, which appears unlikely. In addition, if such a process would be the origin, one then would expect a distribution of the numbers of photons absorbed and thus signal from hemin$^+$ that only partially evaporated its droplet, which is not observed. Thus, the detection of hemin$^+$ likely results from the ejection of the ion from the droplet, similar to what has been observed by the Drabbels group.[19]

To determine what exactly is being ejected from the droplet, the resolution of the TOF measurement needs to be improved and to this end, a TOF spectrometer perpendicular to the flight direction is installed. In this experiment, the doped droplet beam first enters the region between the TOF acceleration plates. The beam is then crossed by the laser beam at 380 nm *via* the multipass setup and a few microseconds after the laser, the plates are pulsed to high voltage and ions are accelerated towards an MCP detector. Only comparatively light species will reach the detector, as heavy droplets have a substantial kinetic energy perpendicular to the acceleration direction. Resulting mass spectra for high and low laser fluence are shown in Fig. 5. The main peak at m/z = 616 u/q results from bare hemin$^+$. At the high mass side, two small peaks, possibly resulting from water adducts are observed. At lower laser fluence (~12 mJ per pulse cm^{-2}) no significant signal at lower masses is observed. At higher laser fluence (~50 mJ per pulse cm^{-2}), peaks at lower masses that result from hemin$^+$ which has lost one or both of its sidechains are observed.

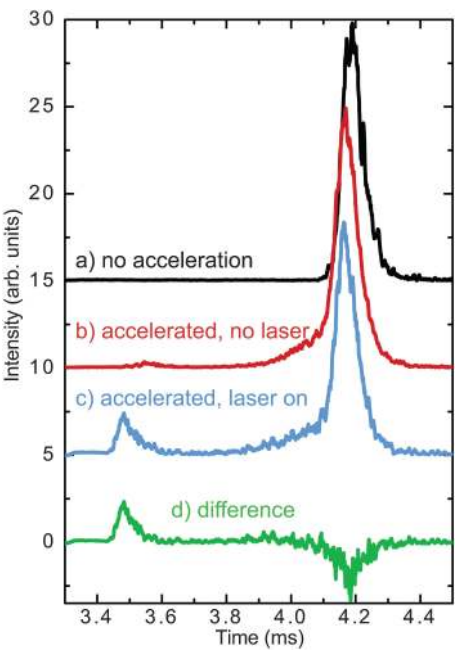

Fig. 4 Time profiles of hemin$^+$ doped droplets at T_{source} = 16 K, monitored using the Daly detector. (a) Profile for the unaccelerated beam, (b) acceleration with 50 V, (c) acceleration with 50 V after laser excitation, (d) difference between traces (b) and (c). The small peak near 3.5 ms results from hemin$^+$ that is ejected from the droplet.

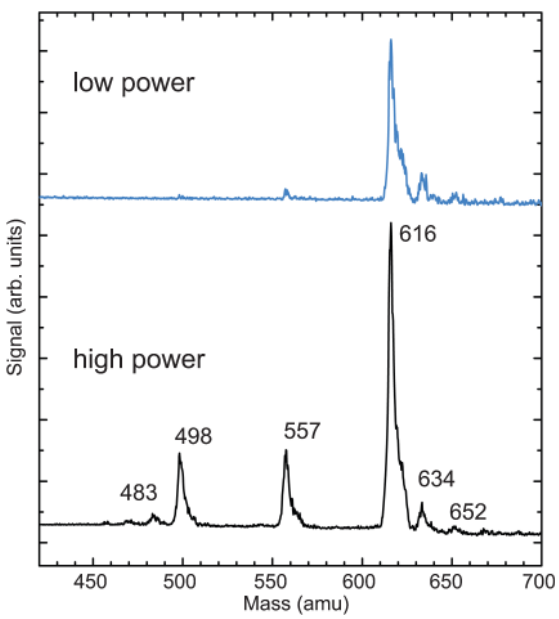

Fig. 5 Bottom (black): time-of-flight mass spectrum for hemin$^+$ at high laser power. Peaks at 557 u and 498 u correspond to loss of one and two CH_2COOH side chains, at 483 u an additional methyl group is lost. Top (blue): same at low laser power without fragmentation.

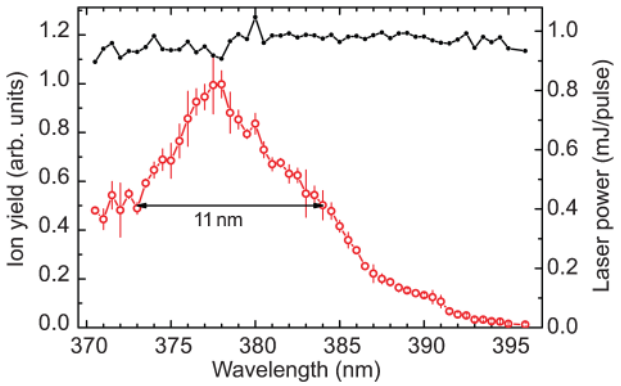

Fig. 6 Red: ejected ions as a function of laser excitation wavelength, normalized to the peak intensity. Black: laser power in mJ per pulse.

The ejected ions can be recorded as a function of laser wavelength to give the spectrum shown in Fig. 6. For this, the laser power is kept low to avoid fragmentation and held constant to within 5%. The spectrum shows a broad and unstructured peak at a position where one expects the well known Soret ($S_2 \leftarrow S_0$) band of hemin to occur.[29,30] Compared to the gas-phase spectrum of hemin$^+$ measured for room-temperature ions,[30] the here presented spectrum is slightly (~3 nm) shifted to the blue and also slightly narrower (FWHM ~11 nm *vs.* ~16 nm). In general, the spectrum is broad and unstructured. This can be attributed to the ultrashort lifetime in the excited state.[31] As is discussed below, the ejection does not appear to be a one-photon process which can affect the shape of the spectrum by, for example, slightly enhancing regions with high absorption cross-sections or higher photon energies. The ejection of ions from droplets after photoexcitation has been observed before,[19] the mechanism for this process, however, remains unclear. To shed some more light on this process, we measured the dependence of the observed ion signal on the laser fluence. The results are shown in Fig. 7. The laser wavelength is set at 378 nm and the droplet source is operated at 15 K, 20 Hz and 65 bar backing pressure. In order to obtain a homogeneous illumination of the droplets, the laser beam is first expanded *via* a telescope to a beam diameter of about 10 mm and then, the central 4 mm diameter part that is cut out *via* an iris is used. Because of this, the laser fluences used in this experiment cannot be directly compared to those used to obtain the data in Fig. 4–6 where the laser beam profile is different. The experimental data are shown as points and clearly, the results are not compatible with a single photon process, of which a best fit is shown as a dotted line. The experimental data can also be modeled by integrating differential equations describing a two photon process shown in eqn (2):

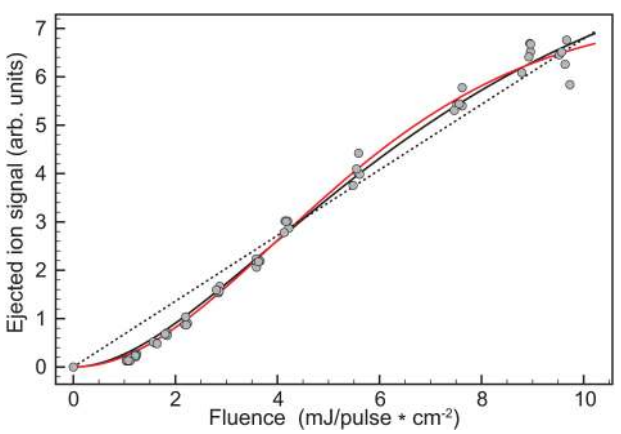

Fig. 7 Points: experimental data. Dotted line: one-photon model. Black: two photon model, no relaxation. Red: two photon model with condensed phase hemin absorption cross-sections and relaxation pathways. See text for details.

$$\mathrm{A} \underset{k_1}{\overset{k_{abs}}{\rightleftharpoons}} \mathrm{B} \underset{k_2}{\overset{k_{abs}}{\rightleftharpoons}} \mathrm{C} \xrightarrow{k_3} \text{ejected ions.} \qquad (2)$$

In this model, k_{abs} is the excitation rate constant, which is the absorption cross-section times the photon flux, k_1 and k_2 describe relaxation processes and k_3 is the rate constant for ejection out of the droplet. *B* and *C* are not meant to indicate electronically excited states of the chromophore, but rather general states of the doped droplets on the way towards ion ejection. k_{abs} is set to be equal for both steps, which appears to be reasonable, as relaxation from an excited state is ultrafast and one can therefore assume that a second photon is absorbed by the molecule after being back in its electronic ground state. A further parameter for a fit to the experimental data is an intensity scaling parameter. Allowing all those parameters to freely vary would lead to linear dependencies and meaningless fit results. Therefore, constraints need to be applied. Shown as a solid black line is a fit obtained when setting $k_1 = k_2 = 0$. Unless being too small, the value of k_3 is then irrelevant, as due to the lack of relaxation pathways, all ions in state C will eventually be ejected. The only adjustable parameter is thus the absorption cross-section of hemin and the fit gives a value of 1.4×10^{-16} cm^2.

That number can be compared to the absorption cross-section in solution. Measurements in $MeOH/CH_2Cl_2$ (50 : 50) as solvent at a concentration of 3 μm M/L yield at 378 nm an extinction coefficient of 2.2×10^5 L (mol cm)$^{-1}$, being equivalent to a cross-section of 8.6×10^{-16} cm^2 per molecule. A fit of the fluence dependence with the above model and the excitation rate constant being fixed to this measured absorption cross-section times the laser fluence is shown as a solid red line in Fig. 7. The relaxation rate constants k_1 and k_2 were forced to be equal and the fit gives a value of 9×10^9 s^{-1}. For k_3, a value that is several orders of magnitude larger than that of k_2 is obtained and the fit is therefore insensitive to the exact value of k_3. The agreement between the experiment and the model described in eqn (2) tells us that at least two photons need to be absorbed for ejection to occur under the experimental conditions employed. The rate constants obtained from the fit appear reasonable, however only an order of magnitude estimate can be obtained, as the fit with the model is to some extent underdetermined. As can be seen from the two fits with a two photon absorption model, the fitted values for the absorption and relaxation rate constants are coupled such that a large absorption cross-section can be compensated by a large relaxation rate and when for illustration of this dependence, the cross-section is doubled to 1.7×10^{-15}, the fitted value for k_1 increases to 2.5×10^{10} s^{-1}.

In the experiment, it is observed that the ejection yield strongly increases with increasing droplet source temperature.

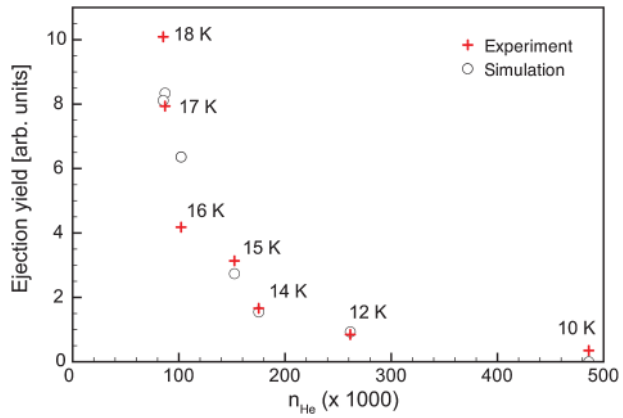

Fig. 8 Number of ejected ions per pulse divided by peak current of droplet pulse *versus* the median of the corresponding droplet size distribution. The laser wavelength is 380 nm and the fluence 0.5 mJ in a 10 mm diameter spot.

In Fig. 8, the ejected ion signal, for normalization divided by the peak droplet signal at the respective temperature, is plotted against the median of the measured droplet distribution at the corresponding temperatures. Red crosses represent data points and open circles a modeling of the data. Clearly, the ejection yield strongly increases with decreasing droplet size. Similar observations were made by Drabbels *et al.*[19] for droplets that are first doped by small neutral molecules and then photoionized, for different photon energies and for much smaller droplet sizes. To obtain some more physical insight, we model the data with the assumption that the ejection yield depends exponentially on the number of helium atoms, $I(n) = A \times \exp(-Bn)$. This expression is multiplied with the experimentally determined log-normal distribution (eqn (1), see also bottom part of Fig. 3) and integrated. The simulated points do not show a smooth behavior, as for their determination the experimental size parameters are used which have, especially at high temperatures, some uncertainty. For the present data, the fitted parameter A has no physical meaning, as the absolute scale for the ejection yield is not known. For B, a value of 3.1×10^{-5} is obtained, *i.e.* the ejection yield drops by $1/e$ every 32 000 helium atoms. In the model, it is implicitly assumed that the ejection yield will approach unity at some droplet size. Where this can however not be obtained, as this information is contained in the parameter A. The observation that ions do get ejected from helium droplets remains puzzling. As has been pointed out before,[19] the mechanism has to be non-statistical, as an equilibration of the energy after excitation but before ejection would lead exclusively to evaporation of helium atoms. The electronically excited states of hemin are known to relax ultrafast to the ground state. It is thus unlikely that ejection occurs due to possibly repulsive interaction of excited states with helium. In line with this, dopant ejection has also been observed for ions in helium droplets after IR excitation.[19,20]

4 Conclusions

The here presented data show that mass/charge selected ions can efficiently be incorporated into helium droplets ranging in size from tens of thousands to millions of helium atoms. In the present implementation, peak droplet currents of up to one picoampere can be obtained, which is sufficient for a wide range of experiments. By performing acceleration experiments on the droplets, the mass distribution can be determined. It is observed that the droplet distributions can be well described by log-normal distributions. The parameters of the distribution primarily depend on the helium stagnation pressure and the source temperature. For the here investigated case of hemin$^+$ in helium droplets, it is observed that excitation with UV light can lead to ejection of the ion from the droplet. Monitoring the ejection yield as a function of excitation wavelength can be used to obtain the UV spectrum of hemin$^+$. For doped droplets with a median size of $\sim$150 000 helium atoms (T_{source} = 15 K), the absorption of two photons at 380 nm is needed for ejection to become efficient. When droplets become smaller, the ejection efficiency is observed to strongly increase. The microscopic mechanism by which ejection occurs is still unclear.

Acknowledgements

We gratefully thank Uzi Even for help and advice with the pulsed droplet source and Waters for providing the QTof mass spectrometer.

References

1 J. Gspann, in *Physics of Electronic and Atomic Collisions*, ed. S. Datz, North-Holland Publishing Company, Amsterdam, 1982, pp. 79–96.
2 S. Goyal, D. L. Schutt and G. Scoles, *Phys. Rev. Lett.*, 1992, **69**, 933–936.
3 R. Fröchtenicht, J. Toennies and A. Vilesov, *Chem. Phys. Lett.*, 1994, **229**, 1–7.
4 F. Stienkemeier and K. K. Lehmann, *J. Phys. B: At., Mol. Opt. Phys.*, 2006, **39**, R127–R166.
5 M. Y. Choi, G. E. Douberly, T. M. Falconer, W. K. Lewis, C. M. Lindsay, J. M. Merritt, P. L. Stiles and R. E. Miller, *Int. Rev. Phys. Chem.*, 2006, **25**, 15–75.
6 J. P. Toennies and A. F. Vilesov, *Angew. Chem., Int. Ed.*, 2004, **43**, 2622–2648.
7 C. Callegari, K. K. Lehmann, R. Schmied and G. Scoles, *J. Chem. Phys.*, 2001, **115**, 10090–10110.
8 S. Grebenev, J. P. Toennies and A. F. Vilesov, *Science*, 1998, **279**, 2083–2086.
9 A. R. W McKellar, Y. Xu and W. Jäger, *Phys. Rev. Lett.*, 2006, **97**, 183401.
10 F. Stienkemeier, J. Higgins, W. E. Ernst and G. Scoles, *Phys. Rev. Lett.*, 1995, **74**, 3592–3595.
11 P. Claas, S. O. Mende and F. Stienkemeier, *Rev. Sci. Instrum.*, 2003, **74**, 4071.
12 A. Lindinger, J. P. Toennies and A. F. Vilesov, *J. Chem. Phys.*, 1999, **110**, 1429–1436.
13 J. D. Close, F. Federmann, K. Hoffmann and N. Quaas, *Chem. Phys. Lett.*, 1997, **276**, 393–398.
14 M. Hartmann, R. E. Miller, J. P. Toennies and A. F. Vilesov, *Science*, 1996, **272**, 1631–1634.
15 M. N. Slipchenko, S. Kuma, T. Momose and A. F. Vilesov, *Rev. Sci. Instrum.*, 2002, **73**, 3600–3605.
16 D. Pentlehner, R. Riechers, B. Dick, A. Slenczka, U. Even, N. Lavie, R. Brown and K. Luria, *Rev. Sci. Instrum.*, 2009, **80**, 043302.
17 D. Pentlehner, C. Greil, B. Dick and A. Slenczka, *J. Chem. Phys.*, 2010, **133**, 114505.
18 N. B. Brauer, S. Smolarek, X. Zhang, W. J. Buma and M. Drabbels, *J. Phys. Chem. Lett.*, 2011, 1563–1566.

19 S. Smolarek, N. B. Brauer, W. J. Buma and M. Drabbels, *J. Am. Chem. Soc.*, 2010, **132**, 14086–14091.
20 X. Zhang, N. B. Brauer, G. Berden, A. M. Rijs and M. Drabbels, *J. Chem. Phys.*, 2012, **136**, 044305.
21 W. Lewis, R. Bemish and R. Miller, *J. Chem. Phys.*, 2005, **123**, 141103.
22 D. Bonhommeau, M. Lewerenz and N. Halberstadt, *J. Chem. Phys.*, 2008, **128**, 054302.
23 F. Bierau, P. Kupser, G. Meijer and G. von Helden, *Phys. Rev. Lett.*, 2010, **105**, 133402.
24 M. Lewerenz, B. Schilling and J. P. Toennies, *Chem. Phys. Lett.*, 1993, **206**, 381–387.
25 U. Henne and J. P. Toennies, *J. Chem. Phys.*, 1998, **108**, 9327–9338.
26 L. F. Gomez, E. Loginov, R. Sliter and A. F. Vilesov, *J. Chem. Phys.*, 2011, **135**, 154201.
27 D.-S. Ahn, F. Filsinger, A. I. Gonzalez-Florez, G. Meijer and G. von Helden, *to be published.*
28 E. L. Knuth and U. Henne, *J. Chem. Phys.*, 1999, **110**, 2664–2668.
29 *The Porphyrins*, ed. D. Dolphin, Academic Press, New York, 1978, vol. III.
30 M. K. Lykkegaard, A. Ehlerding, P. Hvelplund, U. Kad-hane, M.-B. S. Kirketerp, S. B. Nielsen, S. Panja, J. A. Wyer and H. Zettergren, *J. Am. Chem. Soc.*, 2008, **130**, 11856–11857.
31 M.-H. Ha-Thi, N. Shafizadeh, L. Poisson and B. Soep, *Phys. Chem. Chem. Phys.*, 2010, **12**, 14985.